Y. Jus
LAMSID,
UMR CNRS/EDF/CEA No 2832,
1 Avenue du Général de Gaulle,
Clamart cedex 92141, France;
UPMC
Univ Paris 06,
UMR 7190,
Institut Jean Le Rond d'Alembert,
Paris F-75005, France;
CNRS,
UMR 7190,
Institut Jean Le Rond d'Alembert,
Paris F-75005, France

E. Longatte[1]
LAMSID,
UMR CNRS/EDF/CEA No 2832,
1 Avenue du Général de Gaulle,
Clamart cedex 92141, France

J.-C. Chassaing
UPMC
Univ Paris 06,
UMR 7190,
Institut Jean Le Rond d'Alembert,
Paris F-75005, France;
CNRS,
UMR 7190,
Institut Jean Le Rond d'Alembert,
Paris F-75005, France

P. Sagaut
UPMC
Univ Paris 06,
UMR 7190,
Institut Jean Le Rond d'Alembert,
Paris F-75005, France;
CNRS,
UMR 7190,
Institut Jean Le Rond d'Alembert,
Paris F-75005, France

Low Mass-Damping Vortex-Induced Vibrations of a Single Cylinder at Moderate Reynolds Number

The feasibility and accuracy of large eddy simulation is investigated for the case of three-dimensional unsteady flows past an elastically mounted cylinder at moderate Reynolds number. Although these flow problems are unconfined, complex wake flow patterns may be observed depending on the elastic properties of the structure. An iterative procedure is used to solve the structural dynamic equation to be coupled with the Navier–Stokes system formulated in a pseudo-Eulerian way. A moving mesh method is involved to deform the computational domain according to the motion of the fluid structure interface. Numerical simulations of vortex-induced vibrations are performed for a freely vibrating cylinder at Reynolds number 3900 in the subcritical regime under two low mass-damping conditions. A detailed physical analysis is provided for a wide range of reduced velocities, and the typical three-branch response of the amplitude behavior usually reported in the experiments is exhibited and reproduced by numerical simulation.
[DOI: 10.1115/1.4027659]

Keywords: large eddy simulation, fluid structure interaction, vortex-induced vibrations

1 Introduction

Solving multiphysics problems in the context of large scale industrial applications remains a challenge requiring both the use of advanced computational methods with high-fidelity turbulence modeling and high performance computing (HPC) resources. Unsteady flows in very confined areas such as those encountered in steam exchangers and heat generator tube arrays may feature complex dynamical behavior. Each cylinder can lead to Karman vortices and it is possible to observe a jet issuing between the tubes depending on the critical size of cylinder spacing and space confinement.

When flexible effects in tube arrays are taken into account, vortex-induced vibrations (VIV) may deeply affect the dynamical response of the structure. This is one of the numerous possible dynamical mechanisms involved in cylinder arrangements. The analysis of VIV of a single cylinder in an infinite medium without any confinement is investigated in the present work. The cylinder is constrained to move in the lift direction and features under certain circumstances a kind of synchronization of the vortex shedding frequency f_s with the natural frequency of the system f_n. For a given reduced velocity $U^* = U/f_n D$ with U the fluid velocity and D the cylinder section diameter, the amplitude of the cylinder motion and the nature of the mode emission of the vortex shedding are governed by the mass-damping parameter $m^* \xi$ with m^* the ratio between structure mass and displaced fluid mass and ξ the damping ratio.

In the case of low mass-damping, three kinds of amplitude response can be observed in the lift direction, namely, the initial, the upper, and the lower branches [1–3]. Low values of the reduced velocity correspond to the initial branch of the response model. For this regime, the wake flow exhibits two single vortices shed per cycle (2S mode emission) and the mean forces are in phase with the motion of the cylinder. Increasing the reduced velocity gives rise to the upper branch with high amplitude response. The mode transition between these branches is hysteretic. The phase shift between the lift force and the cylinder motion observed during the lock-in is about 180 deg. Higher values of the reduced velocity lead to the small amplitude lower branch. For this regime, the vortex shedding is characterized by a mode with two pairs of vortices shed per cycle (2P mode emission). The transition with the upper branch exhibits an intermittent switching.

Numerous numerical works are devoted to the study of the three-branch response model for low mass-damping problems by means of computational fluid dynamics [4–6]. However,

[1]Corresponding author.
Contributed by the Pressure Vessel and Piping Division of ASME for publication in the Journal of Pressure Vessel Technology. Manuscript received September 23, 2013; final manuscript received May 9, 2014; published online August 19, 2014. Assoc. Editor: Samir Ziada.

accurately reproducing the upper branch response remains very tricky as shown by two-dimensional large eddy simulation (LES) performed by Al-Jamal and Dalton [7] at Reynolds number 8000. Several attempts are devoted to characterizing the lock-in region by means of two-dimensional unsteady Reynolds-averaged Navier–Stokes (2D-URANS) simulations [8,9]. The use of such methods is very attractive because of their flexibility and robustness, but 2D-URANS approaches of VIV at low mass-damping usually fails in describing the correct three-branch response model as observed experimentally for moderate Reynolds numbers. Pan et al. [9] point out the incapacity of 2D-URANS methods to reproduce random disturbances in vortex shedding responsible for the mode transition, resulting in the absence of the upper branch with such approaches. Guilmineau and Queutey [8] investigate several initial conditions for predicting the maximal VIV magnitude responses as reported experimentally by Khalak and Williamson [1]. It is shown that the maximal vibration amplitude is reproduced under specific increasing velocity initial conditions. However, the extent to the synchronization region is strongly underestimated. A relevant numerical model of high amplitude upper branch regime is described by Lucor et al. [10] by means of direct numerical simulation (DNS) through a spectral element approach. The large magnitude response in the lock-in region and the 2P mode emission are clearly observed. The sensitivity to Reynolds number in the range from 1000 to 3000 is investigated in configurations with zero structural damping.

The purpose of the present work deals with the evaluation of LES for computation of VIV of a circular cylinder in an infinite area at moderate Reynolds number. A particular attention is paid to comparison of solutions in the upper branch with available solutions for both zero structural damping and low mass damping. This article is split into three parts. The formulation and the computational procedure are briefly presented in Sec. 2. Section 3 is devoted to VIV analysis at Reynolds number 3900 for two low mass-damping configurations from literature. Finally, computational times and resources for both static and dynamic flow problems are discussed. In the context of the present work, all simulations are carried out at Reynolds number 3900 to enable comparisons with experimental data of Hover et al. [23]. Comparisons with other numerical solutions corresponding to lower values of Reynolds number are also performed in order to contribute to the characterization of branch response dependency according to Reynolds number. A cross analysis of dependency on several parameters is therefore possible including Reynolds number, reduced velocity, mass ratio, and Scruton number.

2 Theoretical Background

In the context of a pseudo-Eulerian formulation involving a moving-grid method for near-moving wall space discretization, the filtered equations governing the dynamical behavior of an incompressible flow can be written as follows:

$$\begin{aligned} &\frac{\partial \bar{u}_i}{\partial x_i} = 0 \\ &\frac{\partial \overline{u_i}}{\partial t} + (\overline{u_i} - v_{gi})\frac{\partial \overline{u_i}}{\partial x_j} = -\frac{1}{\rho}\frac{\partial \bar{p}}{\partial x_i} + \nu\frac{\partial^2 \overline{u_i}}{\partial x_j \partial x_j} - \frac{\partial \tau_{ij}}{\partial x_j} \end{aligned} \tag{1}$$

where v_g represents the grid cell velocity, $\bar{u}$ and $\bar{p}$ the spatially filtered fluid velocity and pressure, ν the kinematic viscosity, and the subgrid-scale tensor $\bar{\bar{\tau}}$ is modeled by the Smagorinsky model, which is based on Germano identity [11] and Lilly minimization [12]. The deviatoric part of the subgrid-scale tensor is given by

$$\tau_{ij} - \frac{1}{3}\tau_{kk}\delta_{ij} = -2\nu_t S_{ij} = -2(C_s\bar{\Delta})^2\|S\|S_{ij} \tag{2}$$

where S_{ij} represents the filtered strain rate tensor, $\|S\| = \sqrt{2S_{ij}S_{ij}}$, and ν_t denotes the subgrid-scale viscosity, $\bar{\Delta}$ is the filter width, and C_s is the Smagorinsky constant ($C_s = 0.065$). Only hexahedral computational cells of volume Ω are considered in the present work and one uses $\bar{\Delta} = 2\Omega^{1/3}$. The term $(1/3)\tau_{kk}\delta_{ij}$ is taken into account in the pressure gradient.

The governing equations for the fluid are solved using a colocated finite volume approach on unstructured mesh with a fractional time step procedure for fluid pressure velocity coupled computation through a projection method [13]. Second order centered schemes in space and time are used. An arbitrary Lagrangian Eulerian approach is introduced to deal with moving solid boundaries. From a mathematical point of view, the introduction of an arbitrary computational reference system means the introduction of a grid mesh impacting convective terms in the momentum equation for incompressible flow, provided that the geometry conservation law [14] is ensured for uniform flow with a first order approximation. Several formulations are possible for the choice of grid velocity dynamics like transfinite mapping strategy, spring analogy or linear elasticity approach. In the present work, an elliptic equation is introduced where variable $\bar{\bar{\lambda}}$ allows cell deformation [15] to be controlled

$$\begin{cases} \nabla \bullet (\bar{\bar{\lambda}}\nabla(v_g)) = 0 & \\ v_g = \dfrac{Du^s}{Dt} & \text{on } \Gamma_{f/s} \\ v_g = 0 & \text{on } \partial\Omega f \backslash \Gamma_{f/s} \end{cases} \tag{3}$$

The assumption that LES filtering commutes with partial derivatives is generally considered to be valid on fixed grids with uniform cell width. This is no longer the case on deforming unstructured grid, but temporal commutation errors are neglected in the present work since they are of second order [16].

At fluid–solid interface, two conditions ensuring continuity of velocity and stress are imposed. The former corresponds to the kinematic no-slip condition and the latter to the equilibrium condition as follows:

$$\begin{cases} u_i = \dfrac{Du_i^s}{Dt} & \text{on } \Gamma_{f/s} \\ \sigma_{ij}n_j = T_{ij}n_j & \text{on } \Gamma_{s/f} \end{cases} \tag{4}$$

where u^s represents the displacement of the interface, D/Dt is the material derivative, and T_{ij} denotes the solid stress tensor. The interfaces between solid and fluid domains are $\Gamma_{s/f}$ and $\Gamma_{f/s}$, respectively. n designates the unit vector normal to the solid domain.

The motion of an elastically mounted rigid circular cylinder freely oscillating in the cross-flow direction is considered. The one degree of freedom dynamics equation of the structure reads

$$m\ddot{y} + c\dot{y} + ky = F_y \tag{5}$$

where y is the displacement in the lift direction, $\dot{y}$ the velocity, $\ddot{y}$ the acceleration of the cylinder, m, c, and k are structural mass, damping, and stiffness, respectively, and F_y represents the action exerted by the fluid in the lift direction. In the framework of rigid motion theory (similarly for linear elasticity), a lagrangian formulation is used for describing the time evolution of the solid kinematics. System remains linear and a Newmark algorithm is involved for time integration.

From a numerical point of view, the major issue is to compute in the same time and in a coupled way flow fields and their interactions with solid displacement. If x designates the physical interfacial fields to be computed in both fluid and solid domains ($x = (u, p)$ and $x = (u^s)$ on $\Gamma_{f/s}$ and $\Gamma_{s/f}$, respectively), this unsteady interfacial problem can be formulated through a nonlinear problem as follows:

$$S_s^{-1}(S_f(x)) - x = 0 \tag{6}$$

where S_s and S_f designate the Steklov–Poincaré operators associated to the involved discrete formulation. Therefore, an iterative method is involved to solve the fully coupled fluid solid system and to look for a solution ensuring continuity conditions through

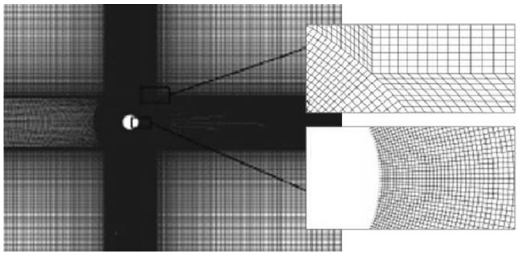

Fig. 1 Representation of near-wall space grid refinement

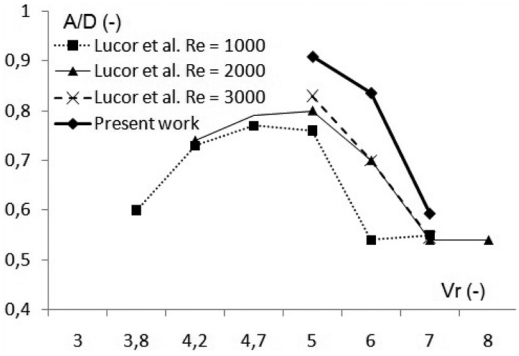

Fig. 2 Dimensionless displacement versus reduced velocity at Re = 3900 and $m^* = 2$ with the present LES compared to DNS solutions of Lucor et al. [10] for Reynolds numbers 1000, 2000, and 3000

the interface at each step of the calculation [15,17–20]. If one considers the coupled problem over a period $[T_N, T_{N+1}]$ of length Δt, a fixed-point iteration is solved as follows:

$$x_{N+1} = S_s^{-1}(-S_f(x_N)) \tag{7}$$

Consistent predictors and correctors are involved for kinematics and stress interface fields to ensure stability and convergence of the solution despite the staggered algorithm. Under-relaxation are introduced to improve the convergence properties of the iterative scheme [17]. As far as convergence properties of iterative solver are concerned, depending on the influence of nonlinear effects, i.e., depending on the range of the physical parameter values to be considered, convergence criteria may be changed in order to reinforce the accuracy of the solution and to tend to converge toward the solution that would be obtained by a fully implicit procedure. Moreover, in the configurations described below, the mass ratio is chosen such that the explicit procedure does not affect numerically the added mass operator [21]. A projection and a condensation methods are employed in order to enable a coupling of the fluid domain interface with a one degree of freedom system modeling the solid dynamics [22].

3 Vortex-Induced Vibrations of a Circular Cylinder

The main objective of this work is to investigate numerically the dynamic response of an elastically mounted cylinder constrained to oscillate transversely to a free stream at low mass-damping, for a Reynolds number defined by $\mathrm{Re} = U_0 D/\nu$ equal to $\mathrm{Re} = 3900$, where U_0 is the inlet velocity. The size of the computational domain is $25D \times 20D$ in the axial and cross-flow directions and the length upstream the cylinder is equal to $15D$. The spanwise length of the domain is set to $4D$. Computations are performed using 32 grid points along the spanwise direction. The total number of cells is equal to 2×10^6. The time step is $\Delta t = 0.001 D/U_0$. The maximal value of the Courant–Friedrichs–Lewy number equals 0.8. A detailed analysis of the

Table 1 Statistical properties of the amplitude response as a function of the reduced velocity at $m^* = 2$ and $m^*\xi = 0$

U^*	A_{mean}/D	A_{max}/D	A_{min}/D	STD
5	0.795	0.909	0.579	0.096
6	0.694	0.836	0.632	0.062
7	0.532	0.593	0.441	0.043

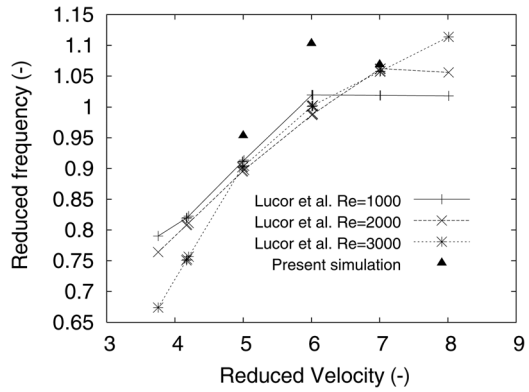

Fig. 3 Reduced frequency f^* versus reduced velocity at Re = 3900 and $m^* = 2$ with the present LES compared to DNS solutions of Lucor et al. [10] for Reynolds numbers 1000, 2000, and 3000

VIV is performed for both zero structural damping and low structural damping $\xi = 0.04$. Figure 1 displays a representation of the grid in the full domain and in the vicinity of the moving cylinder. Cell size is such that the boundary layer smallest structures can be computed. The O-grid, which extends up to four cylinder diameters, includes 300 points equally distributed in the circumferential direction. Near-wall refinement corresponds to a dimensionless radial space grid step of 1 in the boundary layer.

3.1 Case Without Structural Damping. In order to perform comparisons with solutions of Lucor et al. [10], one computes the cylinder vibration amplitude and frequency in the case without any structural damping and with a mass ratio defined by $m^* = 4m/(\rho \pi D^2 L)$ equal to 2. The dynamical response is investigated for three nominal values of the reduced velocity U^* defined by $U^* = U_0/f_n D$. Figure 2 displays a comparison of the highest amplitude response as a function of reduced velocity for the present LES at $\mathrm{Re} = 3900$ with DNS results obtained by Lucor et al. [10] for Reynolds number values included in the range from 1000 to 3000. Figure 2 exhibits A_{max}/D according to reduced velocity in the present work and in Lucor et al. [10]. Table 1 summarizes the values of the mean amplitude A_{mean} evaluated from the average of the peak amplitude of the tenth last periods of oscillation, and also the maximum A_{max}, minimum amplitude A_{min} values and the standard deviation (STD) of A_{mean}.

According to these results, the upper branch response is reproduced numerically for $U^* = 5$ by using LES. Moreover, the sensitivity of the vibration magnitude to the Reynolds number is also retrieved. This sensitivity is pointed out by DNS results obtained by Lucor et al. using a spectral element formulation [10]. It is confirmed here with the proposed LES approach. Using a coarse grid in the spanwise direction does not seem to affect significantly this analysis since in the present work, the computational domain involves 32 grid points in the spanwise direction whereas 128 nodes are employed by Lucor et al. [10]. For each reduced velocity value to be considered, the agreement between LES and DNS is acceptable. The decrease in the amplitude response is correctly predicted as the reduced velocity increases as shown by Fig. 2. According to Table 1, A_{max}/D values are in a relative good

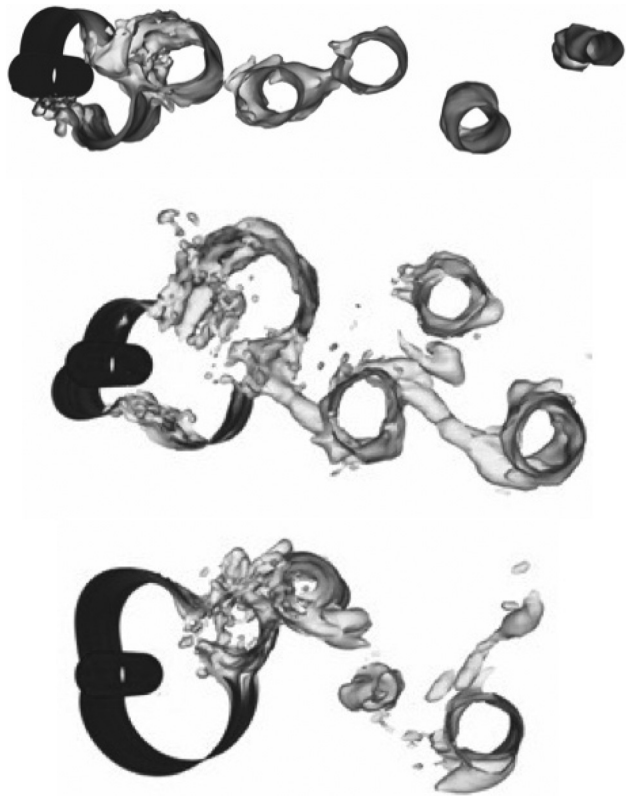

Fig. 4 Isosurface of pressure at 0.1 bar with present LES for reduced velocity equal to 3, 5, and 9 for $m^*=1$, $m^*\xi=0.04$, and Re = 3900

agreement with references and the corresponding coefficient of variation (COV) defined by $\mathrm{COV}=\mathrm{STD}/\mathrm{A}_{\mathrm{mean}}$ ranges from 8% to 12%, which is consistent with the present analysis.

Figure 3 displays the reduced frequency f^* as a function of the reduced velocity. Reduced frequency is defined as the ratio between the frequency of oscillations f_0 and the natural frequency of the system f_n. The lock-in phenomenon is reproduced numerically except at $U^*=6$, where the value of f^* is overestimated by using LES. However, as far as the computational time is concerned, these results tend to show the potential interest of LES for predicting the upper branch response for VIV without any structural damping.

The motivation for comparing solutions obtained for several values of Reynolds number is to show the sensitivity of results to Reynolds number in terms of vibration magnitude level but not in terms of lock-in critical reduced velocity. The weak influence of Reynolds number value on the dynamical and marginal stability of the mechanical system is thus pointed out. The major patterns of the system behavior combining flow and solid dynamics are not changed by the Reynolds number value, except the cylinder dimensionless vibration magnitude A/D whose maximal limit is bounded by one under the considered conditions.

3.2 Case With Low Mass-Damping. In what follows, one considers the numerical parameters used in the experimental study conducted by Hover et al. [23]. Low mass-damping conditions are studied for $m^*\xi=0.04$, where ξ the reduced damping is defined by $c=2m\omega_0\xi$ with ω_0 the system pulsation. The mass ratio is set to $m^*=1$. Several reduced velocities from $U^*=2$ to $U^*=10$ are considered. Figure 4 displays isosurface values at 0.1 bar of pressure for reduced velocity 3, 5, and 9 at Re = 3900. Corresponding flow mode emission in the wake of the cylinder is exhibited. As expected, a 2*S* (two-single vortex) mode emission is observed in the initial branch and a 2*P* (two-pairs of vortices) mode emission occurs in the upper and in the lower branches, which is in

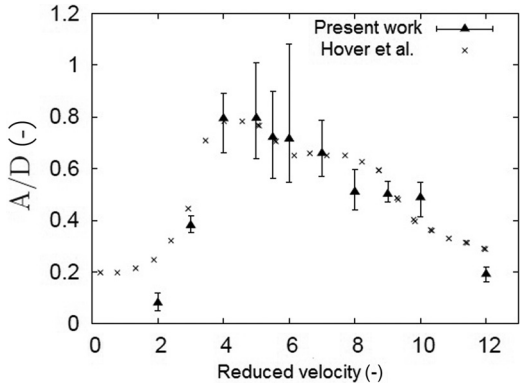

Fig. 5 Comparison of response amplitude according to reduced velocity to the experimental data [23] for Re = 3900, $m^*=1$, and $m^*\xi=0.04$. Mean, minimal, and maximal values of dimensionless displacement.

Table 2 Statistical properties of the amplitude response as a function of the reduced velocity at $m^*=1$ and $m^*\xi=0.04$

U^*	A_{mean}/D	A_{max}/D	A_{min}/D	STD
2	0.081	0.121	0.052	0.019
3	0.380	0.416	0.352	0.02
4	0.794	0.892	0.663	0.052
5	0.795	1.01	0.639	0.056
5.5	0.721	0.898	0.562	0.107
6	0.715	1.08	0.547	0.149
7	0.661	0.821	0.550	0.072
8	0.510	0.598	0.442	0.045
9	0.501	0.549	0.470	0.027
10	0.488	0.546	0.413	0.045
12	0.191	0.219	0.160	0.021

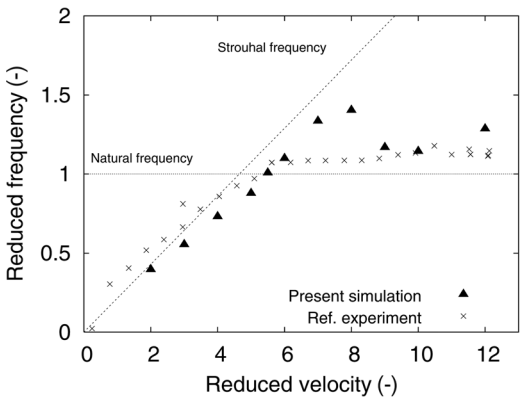

Fig. 6 Reduced frequency versus reduced velocity at Reynolds 3900 ($m^*=1$ and $m^*\xi=0.04$). Comparison between present solution and experimental reference.

accordance with experiment, literature, and theory. This confirms the ability of LES for describing the near-wake of the moving cylinder.

Figure 5 shows that the present LES succeeds in computing the typical branch responses for low mass-damping configurations. Simulations at $U^*=2$ and $U^*=3$ correspond to the initial small amplitude response branch. The high amplitude upper branch can be clearly identified for U^* in the range (4–5). The highest amplitude response is close to those observed experimentally [23]. The reduced velocity range corresponding to the small amplitude lower branch is approximately defined by $U^*=5.5$. The shape of the three-branch response model presents a relatively good quantitative agreement with the model obtained from the experimental

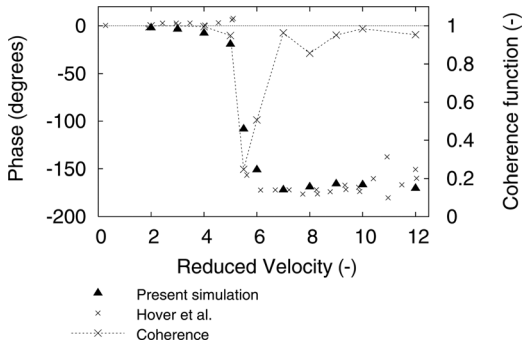

Fig. 7 Coherence and phase angle between lift force and displacement at Reynolds 3900, $m^*=1$, and $m^*\xi=0.04$. Comparison between present solution and experimental reference.

data [23]. Table 2 summarizes the value of the mean amplitude A_{mean} based on the average of the peak amplitude of the tenth last periods of oscillation. The COV = STD/A_{mean} ranges from 6.5% to 23.45%.

The frequency response of the cylinder is plotted in Fig. 6 as a function of the reduced velocity. The expected linear growth of the response is clearly visible below $U^*=7$. However, for reduced velocity 8, the numerical estimate slightly overestimates experimental results of Hover et al. [23]. As far as the lock-in region is concerned, simulations above $U^*=10$ predict a reduced frequency close to one which indicates that the synchronization regime has been reached. The phase angle between lift force and displacement is plotted in Fig. 7 for U^* ranging from 2 to 10. As expected, there is no phase shift between force and displacement as far as the initial and the upper branches are considered [23]. However, the numerical computations exhibit a change in the phase angle from 0 deg to 180 deg representative for the jump from the upper to the lower branch [1]. The range of the reduced velocities $U^*=(5–6)$ characterizing the transition features a good agreement with experimental results [23]. The transition between the initial and the upper branches is characterized by the coherence function relying load and displacement falling to zero as shown in Fig. 7.

At reduced velocity 8, one can notice a slight underestimation of the coherence signal. This tends to show a possible lack of convergence criteria reinforcement in the iterative computational procedure for modeling fluid solid coupled dynamics in this area located near lock-in where inertial effects are responsible for the inversion of energy transfer between flow and cylinder and where a great accuracy is required for numerical schemes to reproduce the flow-driven effects on solid dynamics. This apparent slight numerical weakness is also exhibited in Fig. 6 where the reduced frequency is slightly greater than 1 at reduced velocity 8. In the vicinity of lockin, the convergence criteria should be reinforced, which has not been done in the context of the present work. The full system is solved by using an iterative solver, and the standard convergence is assumed to be reached after three subcycling. In the lock-in area where nonlinearity may be enhanced, ten steps of subcycling may be required to ensure a better convergence of the solution. However, because of the significant computational cost that would be required by additional subcycling, this option has not been chosen in the present work and the solution has been evaluated to be acceptable at least qualitatively since it reproduces with a reasonable accuracy the system behavior in the different branches and it describes correctly the global trends in the transition areas between branches. In spite of this numerical effect, one can conclude that the numerical procedure reproduces the expected behavior of the system with a good quality. Response regimes can also be investigated by means of Lissajou figures plotting lift versus cylinder displacement. A periodogram is used with overlapping using samples of ten periods of vibrational response signal or more. Figure 8(*a*) shows the phase portrait associated with the transition from the initial to the upper branch at $U^*=3$. A nearly periodic behavior is observed for this regime in conjunction with large variations in the lift coefficient. Strongly different responses are obtained during the transition between the upper and lower branches as illustrated in Figs. 8(*b*) and 8(*c*) obtained for $U^*=5$ and $U^*=5.5$, respectively. In contrast with the initial branch, the amplitude of the displacement increases but fluctuations of the lift coefficient are smaller. The intermittent switching in the phase plane portrait of the lift versus displacement is reported for $U^*=5$ (Fig. 8(*c*)). As expected, the lower branch at $U^*=10$ presents a periodic behavior and the resulting displacement and lift variation are smaller than those observed for the other regimes.

Figure 9 displays power spectral densities for reduced velocity $U^*=9$ at two levels $y/D=1$ and $y/D=-1$ for four locations $x/D=1$, 2, 3, 5 in the wake of the cylinder. Two peaks are

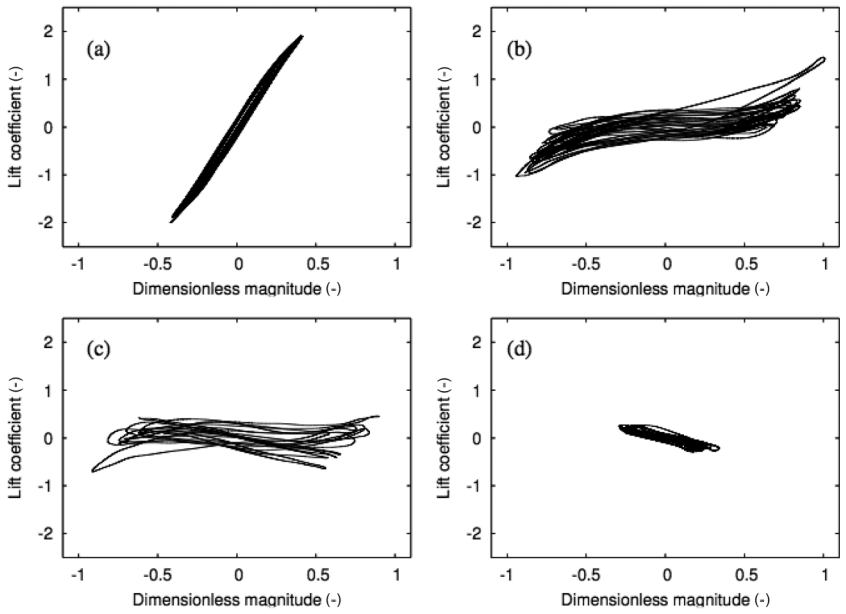

Fig. 8 Phase planes obtained for $m^*=1$ and $m^*\xi=0.04$ at different reduced velocities: (*a*) $U^*=3$, (*b*) $U^*=5$, (*c*) $U^*=5.5$, and (*d*) $U^*=10$

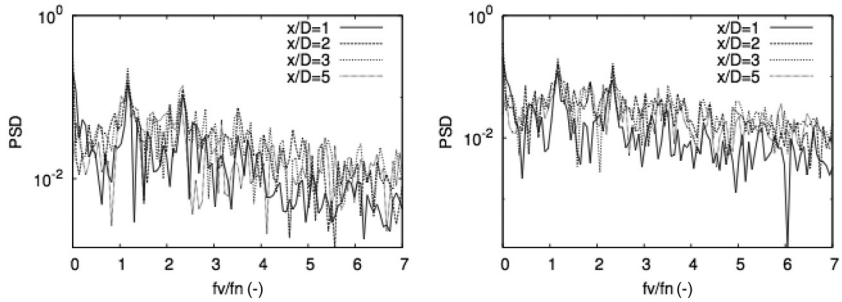

Fig. 9 Power spectral density of cross-flow velocity for reduced velocity $U^* = 9$ at two levels $y/D = 1$ and $y/D = -1$ for four locations $x/D = 1, 2, 3, 5$

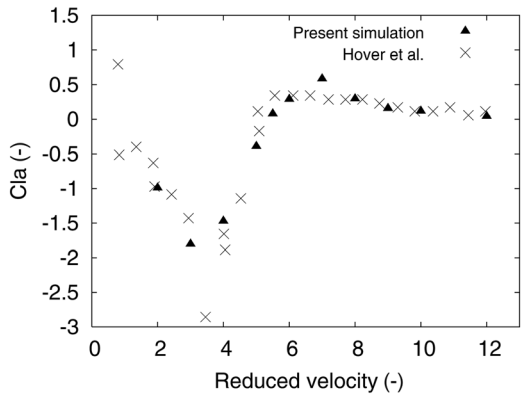

Fig. 10 Lift coefficient in phase with acceleration for $m^* = 1$ and $m^*\xi = 0.04$ with the present LES for Re = 3900

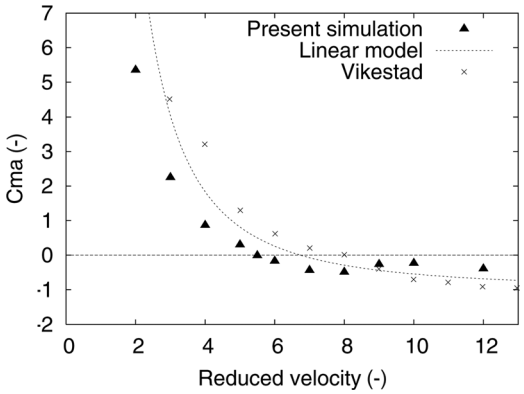

Fig. 11 Variation of mass added coefficient versus reduced velocity for Re = 3900, $m^* = 1$, and $m^*\xi = 0.04$. Present LES compared to linear model and to reference data.

observed showing the presence of a pair of vortices (2P) mode emission as expected for the range of reduced velocity of interest.

Energy exchanges between fluid and structure systems can be analyzed by using the lift coefficient in phase with acceleration C_y [23] through the following dimensionless coefficient C_{la}:

$$C_{la} = \frac{\frac{2}{T_s}\int_{T_s} C_y(t)\ddot{y}(t)dt}{\sqrt{\frac{2}{T_s}\int_{T_s} \ddot{y}^2(t)dt}} \tag{8}$$

where T_s is the sampling period. Figure 10 shows that C_{la} is negative for both the initial and upper branches defined by $U^* < 5.5$. According to Hover et al. [23], this means that the corresponding added mass is positive. Once the lower branch has been reached, the lift coefficient in phase with acceleration vanishes. The solution is globally in good agreement with the experimental data [23].

If one considers the following decomposition of fluid forces:

$$F_f = -m_a\ddot{y} + F \tag{9}$$

where F_f represents the fluid force, m_a the added mass, several models exist to define the component F. In a first approximation, the component F is y-independent and depends only on time. One can write

$$F_f = -m_a\ddot{y} + \frac{1}{2}\rho UDC_L^0 \sin(2\pi Ut/D) \tag{10}$$

with

$$F_f(t) = -\rho\pi D^2 C_{ma}\ddot{y}/4 \tag{11}$$

The added mass coefficient is evaluated by using the following expression derived by Sarpkaya [25]:

$$C_{ma} = m^*\left(\left(\frac{f_{void}}{f_{osc}}\right)^2 - 1\right) \tag{12}$$

where f_{void} and f_{osc} designate, respectively, solid response frequencies without and with fluid.

Figure 11 displays a comparison between the experimental data from Vikestad et al. [24], the linear model and the results from the present simulation evaluated by the expression given by Sarpkaya [25]. The trend is the same as those of linear model and Vikestad et al. work. The coefficient quickly decreases until it becomes negative for $U^* \sim 5.5$. Then, it tends to an asymptotic value of -0.5. The added mass coefficient evaluated numerically is from the opposite sign of lift coefficient in phase with the acceleration [26] and the expected behavior is retrieved. This key result tends to show the efficiency of the proposed LES to reproduce mechanisms responsible for energy exchanges involved by interaction between flow and moving cylinder boundary and their dependency to physical parameters such as reduced velocity, Reynolds number, mass ratio, and structural damping.

4 HPC Resources

Numerical results displayed in the present work are deduced from HPC calculations carried out using 1024 or 2048 processors on BlueGene/L and BlueGene/P supercomputers. In terms of required computational resources for the static case, about 4.5 days are required for 350 physical seconds for the isolated cylinder on 1024 processors (Table 3). For the dynamic case, 1024 processors about eight days are required for computation of VIV over a period range covering ten vortex shedding in the lock-in range. The subcycling procedure involved by the iterative algorithm for

Table 3 HPC performances for static and dynamic configurations

Case	Number of processors	Number of cells	CPU time by iteration	Iteration's number for 10 vortex shedding	CPU time for 10 vortex shedding
Static	1024	2 M	5.8	9661	56,038 s (15h1/2)
Dynamic	1024	2 M (for $U^* = 4, 5, 6$)	15 (Subcycling)	50,000	750,000 s (8d1/2)

fluid-structure coupling is very computational time consuming (Table 3).

5 Conclusions

Incompressible flow around a freely moving cylinder is simulated using LES for a Reynolds number equal to 3900. A wide range of reduced velocities is considered in order to characterize the three-branch response model in the presence of a low mass-damping parameter. First, the mass ratio is set to 2, and numerical predictions are compared with DNS in a case with zero structural damping. Both amplitude displacements and frequencies feature a quantitative agreement with reference numerical results obtained for a Reynolds number from 1000 to 3000. Second, the three distinct branches of the response model are clearly identified for simulations with a mass-damping equal to 0.04. Both the displacement amplitude on the upper branch and the reduced frequency in the lock-in region are compared to experimental results. The phase change between force and displacement corresponding to the transition from the upper to the lower branch is reproduced with accuracy. Third, in the context of HPC, information about computational resources is provided.

Inertial 3D effects responsible for lock-in and described by added mass terms are clearly reproduced. The present work confirms that LES is helpful for better understanding the mechanism responsible for hysteretic transition between initial and upper branches. More generally, the proposed computational approach could be used in the framework of dynamic stability analysis of mechanical systems like cylinder arrangements whose motion patterns are affected not only by inertial effects but also by nonconservative effects described by positive or negative apparent damping to be evaluated numerically.

References

[1] Khalak, A., and Williamson, C. H. K., 1999, "Motions, Forces and Mode Transitions in Vortex-Induced Vibrations at Low Mass Damping," J. Fluids Struct., **13**, pp. 813–851.

[2] Govardhan, R., and Williamson, C. H. K., 2000, "Modes of Vortex Formation and Frequency Response of a Freely Vibrating Cylinder," J. Fluid Mech., **420**, pp. 85–130.

[3] Williamson, C. H. K., and Govardhan, R., 2004, "Vortex-Induced Vibrations," Annu. Rev. Fluid Mech., **36**, pp. 413–455.

[4] Yamamoto, C. T., Meneghini, J. R., Saltara, F., Fregonesi, R. A., and Ferrari, J. A., 2004, "Numerical Simulation of Vortex-Induced Vibration on Flexible Cylinders," J. Fluids Struct., **19**, pp. 467–489.

[5] Singh, S. P., and Mittal, S., 2005, "Vortex-Induced Vibration at Low Reynolds Numbers: Hysteresis and Vortex-Shedding Modes," J. Fluids Struct., **20**, pp. 1085–1104.

[6] Placzek, A., Sigrist, J. F., and Hamdouni, A., 2007, "Numerical Simulation of Vortex Shedding Past a Circular Cylinder at Low Reynolds Number With Finite Volume Technique Part II: Flow Induced Vibrations," ASME Pressure Vessel and Piping Conference, San Antonio, Jul. 22–26, pp. 21–30.

[7] Al-Jamal, H., and Dalton, C., 2004, "Vortex-Induced Vibrations Using Large Eddy Simulation at a Moderate Reynolds Number," J. Fluids Struct., **19**, pp. 73–92.

[8] Guilmineau, E., and Queutey, P., 2004, "Numerical Simulation of Vortex-Induced Vibration of a Circular Cylinder with Low Mass-Damping in a Turbulent Flow," J. Fluids Struct., **19**, pp. 449–466.

[9] Pan, Z. Y., Cui, W. C., and Miao, Q. M., 2007, "Numerical Simulation of Vortex-Induced Vibration of a Circular Cylinder at Low Mass-Damping Using RANS Code," J. Fluids Struct., **23**, pp. 23–37.

[10] Lucor, D., Foo, J., and Karniadakis, G. E., 2005, "Vortex Mode Selection of a Rigid Cylinder Subject to VIV at Low Mass Damping," J. Fluids Struct., **20**, pp. 483–503.

[11] Germano, M., Piomelli, U., Moin, P., and Cabot, W., 1991, "A Dynamic Subgrid-Scale Eddy Viscosity Model," Phys. Fluids, **3**(7), pp. 1760–1765.

[12] Lilly, D., 1992, "A Proposed Modification of the Germano Subgrid-Scale Closure Method," Phys. Fluids, **4**, pp. 633–635.

[13] Archambeau, F., Méchitoua, N., and Sakiz, M., 2004, "A Finite Volume Code for the Computation of Turbulent Incompressible Flows—Industrial Applications," Int. J. Finite Vol., **1**, pp. 1–62.

[14] Lesoinne, M., and Farhat, C., 1996, "A Geometric Conservation for Flow Problems With Moving Boundaries and Deformable Meshes, and Their Impact on Aeroelastic Computations," Comput. Methods Appl. Mech. Eng., **134**, pp. 71–90.

[15] Huvelin, F., 2008, "Couplage de Codes en Interaction Fluide-Structure et Applications aux Instabilités Fluide-Élastiques," Ph.D. thesis, Lille, France.

[16] Moureau, V., Vasilyev, O. V., Angelberger, C., and Poinsot, T. J., 2004, "Commutation Errors in LES on Moving Grids: Application to Piston Engine Flows Center for Turbulence Research Stanfort," Proceedings of the Summer Program.

[17] Longatte, E., Verreman, V., and Souli, M., 2009, "Time Marching for Simulation of Fluid Structure Interaction Problems," J. Fluids Struct., **25**, pp. 95–111.

[18] Piperno, S., 1997, "Explicit/Implicit Fluid/Structure Staggered Procedure With a Structural Predictor and Fluid Subcycling for 2D Inviscid Aeroelastic Simulations," Int. J. Numer. Methods Fluids, **25**, pp. 1207–1226.

[19] Piperno, S., and Farhat, C., 2001, "Partitionned Procedures for the Transient Solution of Coupled Aeroelastic Problems," Comput. Methods Appl. Mech. Eng., **190**, pp. 3147–3170.

[20] Schaefer, M., Heck, M., and Yigit, S., 2007, "An Implicit Partitioned Method for the Numerical Method of Fluid-Structure Interaction," Fluid-Structure Interaction (LNCSE), Vol. 53, H.-J. Bungartz and M. Schäfer, ed., Springer, pp. 171–194.

[21] Causin, P., Gerbeau, J. F., and Nobile, F., 2005, "Added-Mass Effect in the Design of Partioned Algorithms for Fluid Structure Problems," Comput. Methods Appl. Mech. Eng., **194**, pp. 4506–4527.

[22] Maman, N., and Farhat, C., 1995, "Matching Fluid and Structure Meshes for Aero-Elastic Computations: A Parallel Approach," Comput. Struct., **54**(4), pp. 779–785.

[23] Hover, F. S., Techet, A. H., and Triantafyllou, M. S., 1998, "Forces on Oscillating Uniform and Tapered Cylinders in Crossflow," J. Fluid Mech., **363**, pp. 97–114.

[24] Vikestad, K., Vandiver, J. K., and Larsen, C. M., 2000, "Added Mass and Oscillation Frequency for a Circular Cylinder Subjected to Vortex-Induced Vibrations and External Disturbance," J. Fluids Struct., **14**, pp. 1071–1088.

[25] Sarpkaya, A., 2004, "A Critical Review of the Intrinsic Nature of Vortex-Induced Vibrations," J. Fluids Struct., **19**, pp. 389–447.

[26] Gopalkrishnan, R., 1993, "Vortex-Induced Forces on Oscillating Bluff Cylinders," Ph.D. thesis, Departement of Ocean Engineering, MIT, Cambridge, MA.